Compensated State-Space Model of Diode-Clamped MMCs for Sensorless Voltage Estimation

Nima Tashakor, *Member, IEEE*, Yi Zhang, *Member, IEEE*, Shady Banana, Frede Blaabjerg, *Fellow, IEEE*, and Stefan Goetz, *Member, IEEE*

***Abstract*—Modular multilevel converters are well known in the energy sector. Generally, their stable operation is at the expense of numerous sensors, communication burden, and computationally expensive balancing strategies that challenge their expansion to cost-driven applications. Hence, introducing a sensorless voltage-balancing strategy with a simple controller is an attractive objective. Diode-clamped modular multilevel converters (MMCs) offer a simple and effective solution by providing a unidirectional balancing path between two modules through a diode. Ideally, the modulation technique should compensate for the lack of bidirectional energy transfer; hence open-loop operation is possible. Although the sensorless operation is desirable to reduce costs, good knowledge of the modules' voltages for system monitoring, and protection functions still improves operation in some applications or is mandatory in others. However, information should not be at the cost of additional sensors and communication bandwidth. This article develops a compensated state-space model for diode-clamped MMCs to estimate module voltages using an optimal estimator without any direct measurement at module levels. The model considers the effect of the diode-clamped branches and their balancing effect, resulting in 30%–50% reduction in estimation error compared to the conventional models using similar estimators. Simulations and experiments further confirm the provided analysis, where the estimator achieves >97.5% accuracy.**

***Index Terms*—Diode-clamped modules, Kalman filter, modular multilevel converter (MMC), sensorless voltage balancing, state-space model, voltage estimation, voltage estimator.**

I. Introduction

MODULAR multilevel converters (MMCs) are a well-known solution in many high-voltage applications [1], [2]. The main practical advantages compared to other converters are excellent harmonic performance through quantized voltage levels, easy scalability, flexibility due to their modularity, and fault ride-through capability [3], [4]. Such features render MMCs particularly valuable in medium- to high-voltage applications such as high-voltage direct-current transmission, distributed generation, and the basis for energy storage systems and solid-state transformers [5], [6]. However, despite numerous advantages, caveats still need to be addressed, of which balancing and voltage monitoring are among the most critical ones [7], [8].

Under ideal conditions and suitable modulation strategies, MMCs should be stable, and the capacitor voltages should be balanced [9]. However, minor inherent differences in the capacitances, switching behavior, and self-discharge rates of the modules would lead to gradual divergence of the voltages if the modules are not closely monitored or actively balanced through additional hardware [10], [11], [12], [13], [14]. Such active balancing is typically performed in software routines, for which higher functional safety levels necessary for several applications are challenging and cost-intensive [15], [16], [17]. Furthermore, the module-level capacitance determines the dynamics of the module voltage and its imbalance boundary; with the current trend to reduce the module capacitance as much as possible for cost reasons, balancing has to react faster, moving complexity and cost from the power electronics to the peripheral systems [18]. Fast sensors and isolated signaling as part of the monitoring system are responsible for a large share of real-world MMC systems [19].

Diode clamping offers self-balancing capabilities to either add a level of hardware protection to an MMC to achieve higher safety-integrity levels or to reduce the overall cost of the monitoring system [20], [21], [22], [23]. In these topologies, extra diode-clamping paths can create parallel connectivity between neighboring modules if one exceeds the voltage of the other [19], [24]. As the balancing path only has to deal with a fraction of the load current, comparably small low-cost components can be used.

Fig. 1 presents the simplest form of a diode-clamped topology, with the clamping path marked in green. The clamping path forms a balancing backbone, which can even ensure balancing in hardware for high safety-integrity levels. Additionally, they provide the possibility of sensorless operation or can simplify the balancing algorithm considerably and reduce the requirements for high-bandwidth isolated communication as well as the cost of multiple sensors [12], [24], [25], [26].

Manuscript received 27 December 2022; revised 25 March 2023 and 21 May 2023; accepted 29 June 2023. Date of publication 11 July 2023; date of current version 1 September 2023. This work was supported in part by the Federal Ministry of Education and Research of Germany through project "Open6GHub" under Grant 16KISK004 and in part by German Academic Exchange Service (DAAD). *(Corresponding author: Nima Tashakor.)*

Nima Tashakor is with Rheindland-Pfalz Technical Univeristy-Kaiserslautern, 67663 Kaiserslautern, Germany, and also with Duke University, Durham, NC 27708 USA (e-mail: nima.tashakor@rptu.de, nima.tashakorduke.edu).

Yi Zhang is with AAU Energy, Aalborg University, 9220 Aalborg, Denmark (e-mail: yiz@ieee.org).

Shady Banana is with the Technische Universitat Kaiserslautern, 67663 Kaiserslautern, Germany (e-mail: sbanana@rhrk.uni-kl.de).

Frede Blaabjerg is with the AAU Energy, Aalborg University, DK-9220 Aalborg, Denmark (e-mail: fbl@et.aau.dk).

Stefan Goetz is with the Duke University, Durham, NC 27708 USA (e-mail: stefan.goetz@duke.edu).

This article has supplementary material provided by the authors and color versions of one or more figures available at https://doi.org/10.1109/TPEL.2023.3294328.

Digital Object Identifier 10.1109/TPEL.2023.3294328

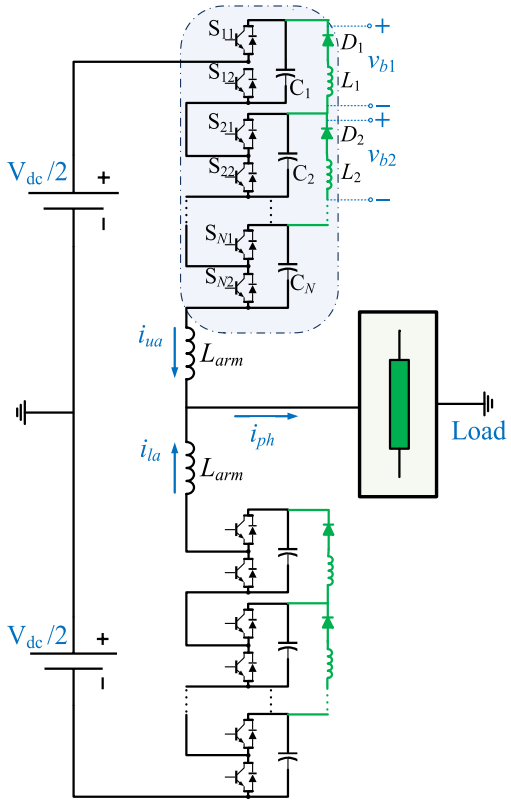

Fig. 1. Single-phase topology of a diode-clamped MMC.

Since the diode only conducts in one direction, the provided balancing path is typically unidirectional [13], [27]. Although more complex clamping topologies exist to create a physical bidirectional balancing path [12], [21], [24], [25], additional diodes, transformers, or even transistors defeat the primary motivation of reduced cost and complexity [28].

A more practical approach can ensure that the required balancing direction complies with the diode conduction path [29]. Such natural balancing direction is closely related to the order by which modules are connected and can easily be achieved by manipulating the modulation reference of the individual modules, such as level-adjusted phase-shifted carrier (LAPSC) modulation without cell-sorting algorithms [12], [26], [30]. Although such methods can also achieve stable open-loop operation, good knowledge of the modules' voltages for system monitoring and protection functions still improves operation in some applications or is mandatory in more critical others [31]. However, higher safety or improved performance should not be at the significant cost of hundreds of more sensors, noticeably higher communication bandwidth, or larger capacitances [32], [33]. Additionally, systems that can guarantee stable open-loop operation can be less susceptible to cyberattacks such as the ones already discussed in the literature [34]. On the other hand, an estimator can provide module voltage information while maintaining the costs and system complexity feasible provided that a sufficiently accurate system model is available [35]. However, there is no available model for diode-clamped MMCs, and the available models for conventional MMCs lead to suboptimal results. Therefore, as we will discuss in Section IV-B, the state-of-the-art estimation techniques for conventional MMC topologies known from the literature [36], [37], [38], [39], [40], [41] achieve inferior results mainly since the available models do not consider the effect of the clamping branch or the balancing control in the diode-clamped MMCs.

This article develops a state-space model for diode-clamped MMCs that considers the effect of the clamping branches and balancing. The proposed model, in combination with an appropriate estimator, can provide a superior estimation of the modules' voltages. Additionally, the developed method is compatible with balancing strategies, such as LAPSC, can offer a more stable estimation under imbalance, and does not require any direct measurement at the module level, considerably reducing communication and measurement costs. Furthermore, we propose a compensation technique for sampling asynchronization that can significantly improve the estimator's accuracy, particularly in lower sampling rates.

The rest of this article is organized as follows. Section II provides a brief introduction to the diode-clamped topology, Section III studies balancing principles, and Section IV proposes the compensated state-space model and its application with an estimator. Simulation and experimental results in Section V verify the performance of the proposed technique. Finally, Section VI concludes this article.

II. Diode-Clamped MMC

Fig. 1 presents the single-phase topology of the diode-clamped MMC containing two identical arms. Multiphase structures repeat the single-phase topology [26], [42].

A. Operation of the Clamping Circuit

Each arm contains N modules, but requires only $(N-1)$ clamping circuits. Each clamping circuit consists of a diode and an inductor in series. The extremely small inductor—as low as few microhenries and therefore with negligible core size [14], [42]—limits the maximum balancing current in the case of high voltage differences between the modules. As the diode should bear only a fraction of the arm current, the cost is minimal. The voltage across the clamping branch (v_{b_i}) includes the diode forward voltage drop (V_{fd}) and the inductance voltage (v_{L_i}) as well as the voltage across the parasitic resistances ($v_{R_{\text{sum}}}$) per

$$v_{b_i} = V_{\text{fd}} + v_{L_i} + v_{R_{\text{sum}}}. \tag{1}$$

Depending on the control signal of the $(i+1)^{\text{th}}$ module as well as the module voltages, three possibilities exist, which are depicted in Table I. When $S_{(i+1)1}$: off and $S_{(i+1)2}$: on, the voltage across the clamping branch depends on the capacitor voltages (V_c) following $v_{b_i} = V_{c_{i+1}} - V_{c_i}$. If $V_{c_{i+1}} \leq V_{c_i} + V_{\text{fd}}$, the branch is open as Fig. 2(a) demonstrates (Mode 1), but if $V_{c_{i+1}} > V_{c_i} + V_{\text{fd}}$, a balancing current flows from C_{i+1} to C_i as Fig. 2(b) illustrates (Mode 2). When $S_{(i+1)1}$: on and $S_{(i+1)2}$: off, the diode is reverse-biased, and, as Fig. 2(c) depicts (Mode 3), the balancing current decays to zero. Assuming negligible resistive elements, the clamping inductor determines the decay rate given as

$$\frac{\mathrm{d}i_D}{\mathrm{d}t} \approx \frac{-(V_{C_i} + V_{\text{fd}})}{L_i} \tag{2}$$

TABLE I
OPERATION MODES OF THE CLAMPING BRANCH

Mode	Switch States	Voltage Condition	Circuit Behavior
1	$S_{(i+1)1}$: off $S_{(i+1)2}$: on	$V_{c_{i+1}} \le V_{c_i} + V_{\text{fd}}$	Open-circuit
2	$S_{(i+1)1}$: off $S_{(i+1)2}$: on	$V_{c_{i+1}} > V_{c_i} + V_{\text{fd}}$	C_{i+1} discharges into C_i (balancing)
3	$S_{(i+1)1}$: on $S_{(i+1)2}$: off	——	Current decays to zero or stays zero

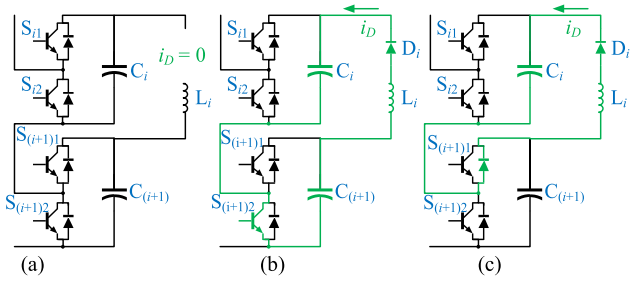

Fig. 2. Different operation modes of the diode-clamped modules. (a) $\boldsymbol{V_{c_{i+1}} \le V_{c_i} + V_{\text{fd}}}$ (Mode 1). (b) $\boldsymbol{V_{c_{i+1}} > V_{c_i} + V_{\text{fd}}}$ (Mode 2). (c) $\boldsymbol{S_{(i+1)2}}$ turns OFF (Mode 3).

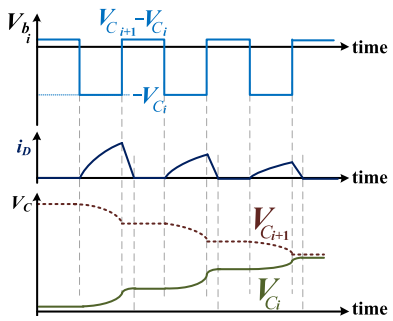

Fig. 3. Intuitive balancing process for balancing of two modules through the clamping branch.

where i_D is the clamping current.

Large imbalances between two modules can require multiple sequences of Modes 2 and 3 until the voltage difference of the modules is cleared ($V_{c_{i+1}} - V_{c_i} \le V_{\text{fd}}$). Fig. 3 illustrates an intuitive representation of this situation. The analysis can be extended to all of the modules in an arm as following:

$$V_{c_1} + V_{\text{fd}} \ge \ldots \ge V_{c_{(N-1)}} + \text{V}_{\text{fd}} \ge V_{c_N}. \tag{3}$$

B. Circuit Analysis

The equivalent electrical circuit when $S_{(i+1)2}$: on and $V_{c_{i+1}} > V_{c_i} + \text{V}_{\text{fd}}$ is a second-order RLC circuit [24], [26]. Based on Kirchhoff's voltage law and after some manipulations, a second-order differential equation can be derived as

$$\frac{\text{d}^2 i_D\,(t)}{\text{d}t^2} + \frac{R_{\text{sum}}}{L_i}\frac{\text{d}i_D\,(t)}{\text{d}t} + \frac{1}{L_i C_e} i_D(t) = 0. \tag{4}$$

The equivalent voltage is $V_{\text{diff}} = V_{c_{i+1}} - V_{c_i}$, and the equivalent capacitance $C_e = 0.5C_i = 0.5C_{i+1}$, $R_{\text{sum}} = R_{C_{i+1}} + R_{L_i} + R_{C_i} + R_{D_i} + R_{S_{(i+1)2}}$ is the sum of all the resistive elements.

Applying Laplace transformation and solving it results in system roots per

$$P_{1,2} = -\frac{R_{\text{sum}}}{2L_i} \pm \sqrt{\frac{R_{\text{sum}}^2}{4L_i^2} - \frac{1}{L_i C_e}}. \tag{5}$$

The equivalent resistance R_{sum} is comparably small; hence, the current will be a damped oscillation which is given by

$$i_D(t) = \frac{V_{\text{diff}}}{\sqrt{\frac{L_i}{C_e} - \frac{R_{\text{sum}}^2}{4}}}\, e^{-\alpha t} \sin \omega_d t \tag{6}$$

where the damping factor $\alpha = \frac{R_{\text{sum}}}{2L_i}$, and the frequency of the oscillation is $\omega_d = \sqrt{\frac{1}{L_i C_e} - \frac{R_{\text{sum}}^2}{4L_i^2}}$. As the diode cannot conduct in reverse, the clamping current can only follow (6) for the first positive half-cycle, and then it stays at zero.

Assuming the maximum permissible voltage difference between modules is $V_{\text{diff\_max}}$, the maximum current amplitude of the diode ($I_{\text{D,max}}$) follows:

$$I_{\text{D,max}} \le \frac{V_{\text{diff\_max}}}{\sqrt{\frac{L_i}{C_e} - \frac{R_{\text{sum}}^2}{4}}}. \tag{7}$$

Therefore, solving for L_i, as long as the inductor follows

$$L_i \ge \left(\frac{R_{\text{sum}}^2}{4} + \frac{V_{\text{diff\_max}}^2}{I_{\text{D,max}}^2}\right) C_e \tag{8}$$

the current of diode D_i is within its rating [26]. Additionally, it is possible to reduce the diode's current rating by increasing the inductor's size. However, a higher inductance value reduces the balancing speed [14]. On the other hand, the maximum permissible voltage difference depends on the balancing technique, tolerance of the capacitors, and the load current [19].

III. PHASE-SHIFTED CARRIER MODULATION

The conventional phase-shifted carrier (PSC) modulation compares a reference waveform (modulation index) with carriers that are phase-shifted with respect to each other. In PSC modulation, each carrier uniquely corresponds to one module in the arm, and the phase shift between two successive carriers is fixed to $\frac{2\pi}{N}$. Under ideal conditions, PSC should reach a stable operating point [7]. However, the system gradually diverges from the intended operation point if no balancing mechanism exists [43].

A diode-clamped circuit can ensure that condition (3) is always maintained, but the voltages only converge if the balancing current flows at all times from the bottom modules in the arm to the upper ones. Although various balancing algorithms expose different behaviors and (dis)advantages, almost all of them ensure a correct balancing direction by manipulating the effective conduction time of the modules [12], [42]. Even closed-loop methods, such as cell sorting, implement a similar measure. Hence, the following analysis focuses on the general effect of the balancing algorithms.

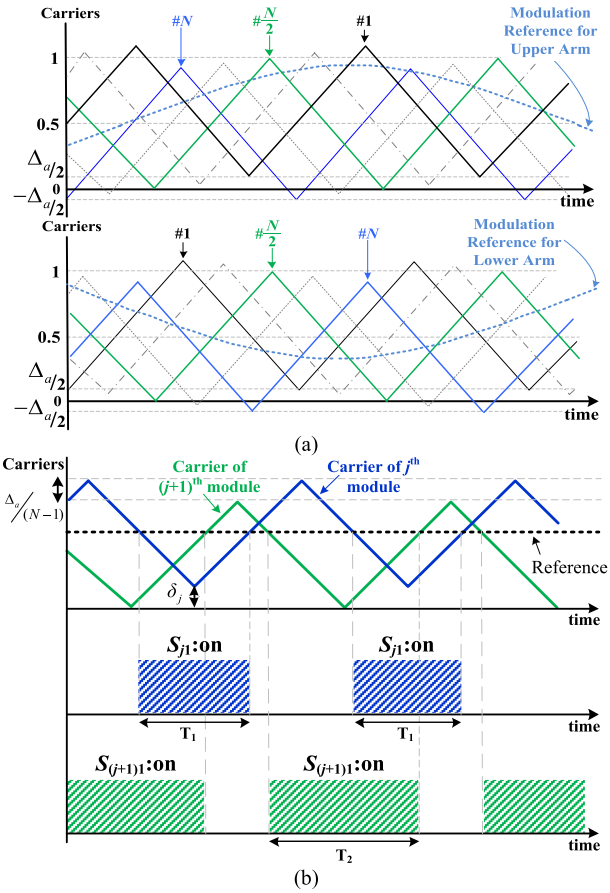

Fig. 4. Intuitive representation of the LAPSC (a) carrier placement in upper and lower arms. (b) Effect of level adjustment on the pulsewidth.

A. Study of Balancing Method

The pulsewidth can be manipulated per module by introducing a slight offset to the modulation reference. Alternatively, such an offset can be a vertical level adjustment in the corresponding carriers, as Fig. 4 intuitively depicts. Both cases cause almost no computational effort, which increases the appeal of the diode-clamped MMCs. A positive vertical level adjustment (for the ith carrier, $\delta_j > 0$) reduces the average duration that the module is connected in series and a negative level adjustment ($\delta_j < 0$) increases the average duration of the series intervals.

Regardless of the balancing method, the arm average current is positive, and shorter durations with series connections reduce the module charge and vice versa. Subsequently, a zero adjustment (in the carriers) or offset (in the individual modulation indices) leads to all modules having the same average series connection duration. If δ_j represents the introduced positive vertical adjustment of jth carrier (or a negative offset in the modulation reference), $\delta_1 \geq \delta_2 \geq \cdots \geq \delta_N$ ensures a bottom-to-top balancing direction at all times. Without lack of generalization, considering the upper arm, the effective modulation index (m_j) for the jth module with $\delta_{u,j}$ is

$$m_{u,j} = \frac{1 - m_a \sin(\omega t)}{2} - \delta_{u,j} \tag{9}$$

where m_a is the normalized amplitude of the phase a.

The effective modulation index ($m_u(t)$) for the complete arm is the average of all the individual m_j values as follows:

$$m_u(t) = \frac{1 - m_a \sin(\omega t)}{2} - \frac{\sum_j^N \delta_{u,j}}{N}. \tag{10}$$

Defining the adjustments for the jth module in the upper arm per

$$\delta_{u,j} = \Delta_a \left(\frac{1}{2} - \frac{j-1}{N-1} \right) \tag{11}$$

results in a zero average for the term corresponding to the adjustment in (10). Hence, the arm voltage is unaffected. Δ_a in (11) is the level adjustment between the first and last carriers of the arm.

Since the balancing direction in the lower arm must also be from bottom to top, $\delta_{l,j}$ should be equal to $\delta_{u,j}$ following (11). However, the carrier orders (phase shifts) in the upper and lower arm should be mirrored at the point where they are connected. The symmetry ensures that at each instant the effects of the balancing effort (e.g., level adjustments) on the voltage of phase a are zero. Hence, the vectors of phase shifts for the upper and lower arm should be

$$\phi_u = \left[0. \frac{2\pi}{N}, \frac{4\pi}{N} \cdots \frac{2\pi(N-1)}{N} \right]^T \tag{12}$$

and

$$\phi_l = \left[\frac{2\pi(N-1)}{N}, \frac{2\pi(N-2)}{N}, \ldots, 0 \right]^T. \tag{13}$$

Based on the symmetry and assuming identical clamping branches with sufficiently large switching frequencies, the average clamping current of the jth clamping branch in the upper arm follows:

$$i_{b_j,u}(t) = \max\left(\frac{1 + m_a \sin(\omega t)}{2} i_u(t) \Delta_a \frac{(N-j)\, j}{N-1}, 0 \right) \tag{14}$$

where $j = 1, \ldots, N-1$ and i_u is the upper arm current. The $\max(.)$ function shows the clamping branch conducts only in the positive direction. Similarly, the clamping current equation for the lower arm is

$$i_{b_j,l}(t) = \max\left(\frac{1 - m_a \sin(\omega t)}{2} i_l(t) \Delta_a \frac{(N-j)\, j}{N-1}, 0 \right). \tag{15}$$

Although a symmetrical definition of the adjustments using (11) can help to reduce the effects of balancing on the load side, many of the balancing strategies do not follow such conventions. Nevertheless, the operating principles of the balancing algorithms remain unchanged.

Whereas the average value of the arm current is always positive, higher harmonic content, namely first-order and second-order components, can result in instances where the arm current is negative, which combined with the open-loop balancing techniques can reduce the balancing efficiency. Therefore, an improved level-adjustment control follows

$$\delta_{u,j} = \operatorname{sgn}(i_{\text{arm},u}) \Delta_a \left(\frac{1}{2} - \frac{j-1}{N-1} \right) \tag{16}$$

which maintains all the previous advantages in addition to improved efficiency.

Although cell-sorting algorithms are not necessary, the sign of the arm current must be closely monitored to control the level adjustment according to (16). The read-out of the sign of the arm current needs at least two updates per fundamental cycle. Proposing a balancing method is not the main contribution of this article, and the compensated model for diode-clamped MMCs in the next section applies to both open-loop and closed-loop balancing techniques.

IV. Proposed State-Space Model and Estimator

A. Compensated State-Space Model

Inherent inter-dynamics of the system introduced by the clamping branch as well as the nonuniform distribution of the parameters (such as the capacitance) complicates the derivation of a complete model for a diode-clamped MMC to the point where only numerical solutions are viable. Additionally, the available analytical simplifications for conventional MMCs will not lead to accurate results, mainly due to the effect of the balancing modulation as well as the clamping branch. Therefore, we extend the conventional model of the MMC to account for both clamping and balancing efforts and then show the application of the model using an optimal estimator (e.g., Kalman filter) to determine the voltage of each module.

The output voltage of the arm based on the module voltages and their states is

$$V_{\text{arm}} = \sum_{j=1}^{N} V_{c_j} S_{j1} = \boldsymbol{V_c^T} \times \boldsymbol{S}_1 \tag{17}$$

where $\boldsymbol{V_c}$ is the vector of module voltages in one arm and $\boldsymbol{S}_1$ is the vector of the upper switches in each module in the same arm with S_{j1} representing its jth element.

The dynamics of the capacitor voltage of an inserted module follows

$$\dot{V}_{c_j} = \mathrm{S_{j1}} \frac{i_{\text{arm}}}{C_j} \tag{18}$$

where C_j is the capacitance of the jth module in the arm. Applying forward Euler discretization leads to

$$V_{c_j}^{(k)} = V_{c_j}^{(k-1)} + \dot{V}_{c_j}^{(k-1)} T_s \tag{19}$$

where T_s is the sampling period. Substituting (18) into (19) results in

$$V_{c_j}^{(k)} = V_{c_j}^{(k-1)} + \mathrm{S_{j1}^{(k-1)}} \frac{T_s}{C_j} i_{\text{arm}}^{(k-1)} \tag{20}$$

and the arm voltage can be written as

$$\boldsymbol{V_c^{(k)}} = \boldsymbol{V_c^{(k-1)}} + \mathbf{S_1^{T^{(k-1)}}} \times \mathbf{I} \times \frac{T_s}{\mathbf{C}} i_{\text{arm}}^{(k-1)} \tag{21}$$

where the vector $\boldsymbol{V_c^{(k)}} = [V_{c_1}^{(\mathrm{k})}, V_{c_2}^{(\mathrm{k})}, \ldots, V_{c_N}^{(\mathrm{k})}]^T$ is the states' vector, $\boldsymbol{S}_1(k-1)$ is a vector containing the switching signals of the modules ($\mathrm{S_{j1}}(k-1)$), $\mathbf{I}$ is the identity matrix, and the vector $\frac{T_s}{\boldsymbol{C_j}}$ is a fixed vector that can be written as

$$\frac{T_s}{\boldsymbol{C_j}} = \left[\frac{T_s}{C_1}, \frac{T_s}{C_2}, \ldots, \frac{T_s}{C_{\mathrm{N}}}\right]^T \tag{22}$$

and can be precalculated. Additionally, the $\frac{T_s}{\boldsymbol{C_j}}$ vector turns into a constant coefficient if all the capacitances are identical.

Hence, the average state-space model of the module voltages follows

$$\boldsymbol{V_c^{(k)}} = \boldsymbol{A_{ss}} \boldsymbol{V_c^{(k-1)}} + \boldsymbol{B_{ss}} i_{\text{arm}}^{(\mathrm{k-1})} + \boldsymbol{w}^{(k)} \tag{23}$$

$$V_{\text{arm}}^{(k)} = \boldsymbol{C_{ss}} \boldsymbol{V_c^{(k)}} + v^{(k)} \tag{24}$$

where the state matrices are $\boldsymbol{A_{ss}} = \mathbf{I}$, $\boldsymbol{B_{ss}} = \boldsymbol{S_1^{T^{(k-1)}}} \times \mathbf{I} \times \frac{T_s}{C_u}$, $\boldsymbol{C_{ss}} = \mathbf{S}_1^{(k)}$, and $\boldsymbol{D_{ss}} = 0$. Additionally, $\boldsymbol{w}(k)$ and $v(k)$ are the modeling and measurement noises, respectively.

In (23) and (24), the effect of the balancing routine on individual modules (e.g., level adjustment for [42], conduction time for [26], or switching delays [12]) are partially considered assuming sufficiently high sampling rates, which leads to increasing the voltage of the lower modules in the arm and decreasing the upper ones. This effect is mainly because any balancing effort will directly affect the $\boldsymbol{S}_1^{(k)}$ vector. Nevertheless, without considering the effect of the clamping branch leading to exchanging energy among modules, the model is inadequate.

Two clamping branches connect each module to the previous (can only discharge said module) and the next modules (can only charge said module) except the first and last modules. Rewriting (19) while considering the effect of these two clamping branches, we arrive at

$$\begin{aligned} V_{c_j}^{(k)} = & \left(1 - \frac{T_s}{2L_jC_j} \left(\begin{array}{c} b_j \left(1 - \mathrm{S_j^{(k-1)}}\right) + \\ b_{(j+1)} \left(1 - \mathrm{S_{(j+1)}^{(k-1)}}\right) \end{array} \right) \right) V_{c_j}^{(k-1)} \\ & + \frac{b_j T_s}{2L_jC_j} \left(1 - \mathrm{S_j^{(k-1)}}\right) V_{c_{(j-1)}}^{(k-1)} \\ & + \frac{b_{(j+1)} T_s}{2L_jC_j} \left(1 - \mathrm{S_{(j+1)}^{(k-1)}}\right) V_{c_{(j+1)}}^{(k-1)} + \frac{T_s}{C_j} \mathrm{S_j^{(k-1)}} i_{\text{arm}}^{(k-1)} \end{aligned} \tag{25}$$

where $S_j = S_{j1}$, and b_j is a variable that according to the switching frequency and modulation reference calculates the average time that the clamping path is forward-biased

$$b_j = \begin{cases} (1 - m_a)\, T_{\text{sw}}, V_{(j+1)} > V_j \\ 0, V_{(j+1)} \leq V_j \end{cases}. \tag{26}$$

Consequently, the compensated state-space model can be rewritten as

$$\boldsymbol{V_c^{(\mathrm{k})}} = \boldsymbol{A'_{ss}} \boldsymbol{V_c^{(\mathrm{k-1})}} + \boldsymbol{B_{ss}} i_{\text{arm}}^{(\mathrm{k-1})} + \boldsymbol{w}^{(k)} \tag{27}$$

$$v_{\text{arm}}^{(k)} = \boldsymbol{C_{ss}} \boldsymbol{V_c^{(k)}} + v^{(k)} \tag{28}$$

where $a'_{pq} \in \boldsymbol{A'_{ss}}$ is the element in the pth row and the qth column. The value of a'_{pq} for all q, p except the first and last

module (i.e., $\forall p, q | p \neq 1, N$) follows

$$a'_{pq} = \begin{cases} \frac{b_p T_s}{2L_p C_p}\left(1 - \mathrm{S}_p^{(k-1)}\right), q = p-1 \\ 1 - \frac{T_s b_p\left(1-\mathrm{S}_p^{(k-1)}\right)}{2L_p C_p} - \frac{T_s b_{(p+1)}\left(1-\mathrm{S}_{(p+1)}^{(k-1)}\right)}{2L_p C_p}, q = p \\ \frac{b_{(p+1)} T_s}{2L_p C_p}\left(1 - \mathrm{S}_{(p+1)}^{(k-1)}\right), q = p+1 \\ 0, \text{else} \end{cases}. \tag{29}$$

If $p = 1$, then $\forall q \in (1, \ldots, N)$

$$a'_{1q} = \begin{cases} 1 - \frac{T_s b_{(p+1)}}{2L_q C_q}\left(1 - \mathrm{S}_{(p+1)}^{(k-1)}\right), q = 1 \\ \frac{T_s b_{(p+1)}}{2L_p C_p}\left(1 - \mathrm{S}_{(p+1)}^{(k-1)}\right), q = 2 \\ 0, \text{else} \end{cases} \tag{30}$$

and for $p = N$ and $\forall q \in (1, \ldots, N)$, a'_{Nq} follows

$$a'_{Nq} = \begin{cases} \frac{T_s b_p}{2L_p C_p}\left(1 - \mathrm{S}_p^{(k-1)}\right), q = N-1 \\ 1 - \frac{T_s b_p}{2L_p C_p}\left(1 - \mathrm{S}_p^{(k-1)}\right), q = N \\ 0, \text{else} \end{cases}. \tag{31}$$

The hardware constraints can prevent sufficiently high sampling rates required in the case of high dynamics or highly imbalanced systems. With a low sampling rate or due to asynchronized sampling, the small balancing efforts can be overlooked and lead to an increased error.

Averaging the modulation index of each module in one cycle of the output voltage results in

$$\bar{m}_{u,j} = \frac{1}{2} - \delta_{u,j} \tag{32}$$

which ideally should reflect the average value of the $S_{1j}(t)$ in one cycle. However, due to low sampling frequencies, high delays in the measurements, or asynchronized sampling (i.e., one state of a module is observed more than the other state), it is possible that the average of the discrete values of $S_{1j}(k)$ per

$$\bar{S}_{j1} = \frac{1}{f_s} \sum_{z=k}^{k-f_s} S_{j1}(z) \tag{33}$$

is not equal to $\bar{m}_{u,j}$, which means the balancing effort is not calculated correctly in the model. Therefore, to compensate for the negative effect of sampling, an additional term can be added to the model by defining a compensated state vector ($\boldsymbol{S}'_1$) according to

$$\boldsymbol{S}'_1(k) = \boldsymbol{S}_1(k) - \left(\bar{\boldsymbol{S}}_1 - \bar{\boldsymbol{m}}_{\boldsymbol{u}}\right). \tag{34}$$

In (34), $\bar{\boldsymbol{S}}_1$ is the vector of the averaged switch states in one fundamental cycle, and it is constantly updated through a sliding window at each iteration. $\bar{\boldsymbol{m}}_{\boldsymbol{u}}$ is the vector of the expected switch states which can be easily calculated for each module per (9). Substituting $\boldsymbol{S}'_1(k)$ in (23) and (24) in (27) and (28) results in a model that can consider the balancing efforts more accurately.

B. Estimation Algorithm

In the last step, an estimation algorithm is integrated with the proposed state-space model to estimate the voltages of the modules [44]. We select a Kalman filter as a prime example of an optimal estimator to verify the performance of the developed model. Table II lists the pseudo-code of the Kalman filter algorithm used to estimate the module voltages. However, other state-of-the-art estimators can be accordingly implemented with the proposed model, and the Kalman filter is only an example used for a quantitative comparison between the conventional and compensated models.

TABLE II
KALMAN FILTER FOR ESTIMATING THE MODULE VOLTAGES OF THE MMC

STEPS		
STEP 0	Initialization	$\hat{\boldsymbol{V}}_c^{(k-1)}, \mathbf{P}^{(0)+}, \boldsymbol{Q}, R$
STEP 1	Projection	$\boldsymbol{V}_c^{(k)-} = \boldsymbol{A}'_{ss}\boldsymbol{V}_c^{(k-1)+} + \boldsymbol{B}_{ss} i_{arm}^{(k-1)}$ $\boldsymbol{P}^{(k)-} = \mathbf{P}^{(k-1)+} + \boldsymbol{Q}$
STEP 2	Calculate KF gain	$\boldsymbol{K}_{\mathbf{g}}^{(k)} = \frac{\boldsymbol{P}^{(k)-}\boldsymbol{C}_{ss}^{T}}{\boldsymbol{C}_{ss}\boldsymbol{P}^{(k)-}\boldsymbol{C}_{ss}^{T} + R}$
STEP 3	Correction	$\boldsymbol{V}_c^{(k)+} = \boldsymbol{V}_c^{(k)-} + \boldsymbol{K}_{\mathbf{g}}^{(k)}\left(v_{arm}^{(k)} - \mathbf{C}_{ss}\boldsymbol{V}_c^{(k)-}\right)$ $\boldsymbol{P}^{(k)+} = \left(\boldsymbol{I} - \boldsymbol{K}_{\mathbf{g}}^{(k)}\boldsymbol{C}_{ss}\right)\mathrm{P}^{(k)-}$
STEP 4	Return to **STEP 1**	$\boldsymbol{V}_c^{(k)+}, \boldsymbol{P}^{(k)+} \Rightarrow \boldsymbol{V}_c^{(k)+}, \boldsymbol{P}^{(k)+}$

In most power electronics systems, the measurement noise as well as the parameter imbalances do not have any type of uniform distribution; therefore, we ultimately should heuristically define the initial covariance matrix ($\boldsymbol{P}$) for the Kalman filter [45]. The measurement noise (R) and modeling error ($\boldsymbol{Q}$) are usually assumed to be independent for each module as well as independent from each other [46]. Therefore, $\boldsymbol{Q}$ is defined as a diagonal matrix, and R as a scalar value, where the initial values should again be set heuristically. However, knowing the effect of each parameter on the estimator's behavior can be of benefit at the beginning of our search. Increasing the value of $\boldsymbol{Q}$ leads to a rapid convergence and prevention of divergence. However, high values of $\boldsymbol{Q}$ will increase fluctuations. On the other hand, reducing the value of $\boldsymbol{Q}$ will reduce the estimation ripple, but also makes the convergence slower and increases the error. Sensitivity to noise can be reduced by increasing R at the cost of slower dynamics.

Comparing the developed model to the conventional one shows that $\boldsymbol{A}'_{\boldsymbol{SS}}$ is not diagonal anymore and has the general form as shown in (35). However, forming the complete $\boldsymbol{A}'_{\boldsymbol{SS}}$ for STEP 1 to perform matrix multiplications is unnecessary. The projected voltage of each module in STEP 1 can be calculated using simple scalar mathematics starting from the first module

$$\boldsymbol{A}'_{\boldsymbol{SS}} = \begin{bmatrix} a'_{11} & a'_{12} & 0 & \cdots & 0 \\ a'_{21} & a'_{22} & a'_{23} & \ddots & \vdots \\ 0 & a'_{32} & a'_{33} & a'_{34} & 0 \\ \vdots & \ddots & \ddots & \ddots & 0 \\ 0 & \cdots & 0 & a'_{N(N-1)} & a'_{NN} \end{bmatrix} \tag{35}$$

In the proposed approach, the estimator is formulated such that each state equation contains a maximum of three state variables and the whole state-space model contains only one output variable. Also, the computations regarding the output equation are entirely simple scalar calculations, which makes

TABLE III
GENERAL COMPARISON OF STATE-OF-THE-ART ESTIMATORS IN THE LITERATURE

Method	Voltage sensors	Advantages and disadvantages
Based on PSO* for conventional MMCs [47]	2	− Computationally extreme; − relatively low accuracy; − very slow convergence speed; − poor performance under rapid variations of operating point
Based on PSO considering parallel modes [48]	2	− Computationally extreme; − very slow convergence speed; − poor performance under rapid variations in operating point; + high accuracy
Based on two-step estimation (model and measurement) [49]	2	− Affected by the sampling delay; − neglects the resistance effect; + computationaly moderate
Based on energy variations in the capacitor [50]	2	− Affected by sampling delay; − neglects the resistance effect; − slow convergence; + computationally moderate
Iterative-based method with delay compensation [37, 51]	≥ 4	− Neglects the resistance effect; − needs at least two extra voltage sensors; − computationaly demanding; + more stable; + considers the sensor behavior on measured signal
Voltage estimation based on Adaline iterative algorithm [38]	2	− Affected by sampling delay; − neglects the resistance effect; − ADALINE method convergence speed is lower than KF; − lower noise sensitivity; + computationaly simple
Based on exponentially weighted recursive least square [52]	2	− Neglects the resistance effect; − neglects the clamping effect; − neglects the balancing effect; + computationally simple; + fast convergence
Based on discrete-time sliding mode observer [53]	2	− Neglects the resistance effect; − neglects the clamping effect; − neglects the balancing effect; − moderate convergance speed; +computationally moderate
Based on KF for conventional MMCs [44]	2	− Affected by sampling delay; − neglects the resistance effect; − neglects the clamping effect; − neglects the balancing effect; + computationally moderate; + good noise sensitivity
EKF for conventional MMCs [54]	2	− Affected by sampling delay; − neglects the clamping effect; − neglects the balancing effect; − computationally demanding; + estimates the arm currents (down not need arm current sensors); + good noise sensitivity; + suitable convergance speed
KF with grouping measurement [55]	≥ 4	− May need higher number of sensors; − computationally extreme; − neglects the resistance effect; − neglects the clamping effect; − neglects the balancing effect; + considers capacitor effect; + more robust; + estimates capacitor value
Based on dual KF for conventional MMCs [41]	2	− Neglects the clamping effect; − neglects the balancing effect; − computationally more demanding; − can be slow in tracking fast variation in capacitor voltage; + Estimates the effective resistance of each module
Voltage estimation based on simplified neural network [32]	2	− Neglects the asynchronous sampling; − neglects the capacitor variation over time; − lower accuracy at dynamic variations; + low computational demand; + considers the balancing effect; + very good accuracy in imbalanced or unstable conditions
KF without arm voltage sensor [56]	1	− Neglects the clamping effect; − neglects the balancing effect; − can be slow in tracking fast variation in capacitor voltage; − sensitive to value of the inductor and resistance in the arm; + lowest number of required sensors; + computationally moderate
Proposed model	2	− Computationally demanding; − neglects the capacitor variation over time (future work); + considers the clamping effect; + considers the balancing effect; + very good accuracy in imbalanced or unstable conditions; + stable with low-frequency switching methods; + compensates for the sampling delay or low-frequency sampling; + applicable with other estimation techniques

* PSO: Particle Swarm Optimization; ** KF: Kalman Filter; *** EKF: Extended Kalman Filter

the computations less demanding for an online implementation in large systems.

In (17), the voltage drops across the parasitic elements are neglected. However, it is also possible to use more accurate models of the arm voltage by considering such voltage drops at the cost of a higher computational burden.

The voltage drops across the components can be easily included in the estimation process by replacing V_{arm} in (17) with V'_{arm} from

$$V'_{\text{arm}} = \sum_{j=1}^{N} (V_{c_j} S_{j1} + V_{j,\text{drop}}) \tag{36}$$

where $V_{j,\text{drop}}$ is the voltage drop across the IGBTs or diodes, as well as the resistive elements calculated using

$$V_{j,\text{drop}} = \begin{cases} S_{j1}\left(V_{d,j1} + R_{d,j1} i_{\text{arm}}\right) \\ +\left(1 - S_{j1}\right)\left(V_{\text{sw},j2} + R_{\text{sw},j2} i_{\text{arm}}\right) & , i_{\text{arm}} \geq 0 \\ -S_{j1}\left(V_{\text{sw},j1} + R_{\text{sw},j1} i_{\text{arm}}\right) \\ -\left(1 - S_{j1}\right)\left(V_{d,j2} + R_{d,j2} i_{\text{arm}}\right) & , i_{\text{arm}} < 0 \end{cases}. \tag{37}$$

Equation (37) can be simplified by assuming identical voltage drops across the diodes (V_d) and IGBTs (V_{sw}) as well as identical corresponding resistive elements, i.e., $V_d = V_{\text{sw}}$, $R_d = R_{\text{sw}}$. Hence, (37) can be simplified to

$$V_{j,\text{drop}} = \text{sgn}\left(i_{\text{arm}}\right)\left(V_{\text{sw}} + R_{\text{sw}} i_{\text{arm}}\right). \tag{38}$$

C. Discussion

It is possible to operate the diode-clamped MMC topology without any direct measurements at the module level to reduce the cost and complexity of the system. However, since the system is running open-loop, the required variations in the duration of the serial connections must be designed for a worst-case scenario, which may not be an optimum solution regarding added losses. Additionally, in many applications, monitoring and protection requirements would still necessitate tracking all the modules' voltages.

Many estimation techniques that can track the voltage of each module are available for conventional MMCs [1], [39]. However, since they do not consider the effect of the clamping branch, none apply to a diode-clamped MMC without significant errors. Additionally, none consider the effect of the balancing algorithms. Table III offers an overview of the state-of-the-art in comparison with the proposed technique.

As main advantages, the presented method includes the balancing routine as well as the influence of the clamping branch on the voltages, proposing a technique to compensate the effect of sampling, which is neglected in other methods; furthermore, the

TABLE IV
PARAMETERS FOR SIMULATION AND EXPERIMENTS

Parameters		Simulation	Experimental
Rated Power		$P_{ac} = 1.14$ MW	$P_{ac} = 2$ kW
Load Inductor		$L_L = 0.1$ mH	$L_L = 0.1$ mH
Module rated voltage		$V_{sm} = 1.2$ kV	$V_{sm} = 45$ V
DC link voltage		$V_{dc} = 9.6$ kV	$V_{dc} = 230$ V
Number of modules		16	10
Arm inductance		$L_{arm} = 5$ mH	$L_{arm} = 2$ mH
Arm Resistor		$R_{larm} = 50$ mΩ	$R_{larm} = 20$ mΩ
Carrier frequency		$f_c = 2$ kHz	$f_c = 2$ kHz
Sampling/Update frequency		$f_s = 10$ kHz	$f_s = 10$ kHz
Output frequency		$f = 50$ Hz	$f = 50$ Hz
Modules	Capacitance	$C_{cap} = 6$ mF	$C_{cap} = 2.5$ mF
	Capacitor resistor	$R_{cap} = 2$ mΩ	$R_{cap} = 2$ mΩ
Modulation index		$m_a = 0.5$~0.95	$m = 0.9$
Clamping circuit	Inductance	$L_{ld} = 10$ µH	$L_{ld} = 1$ µH
	Resistor	$R_{ld} = 0.5$ mΩ	$R_{ld} = 0.5$ mΩ

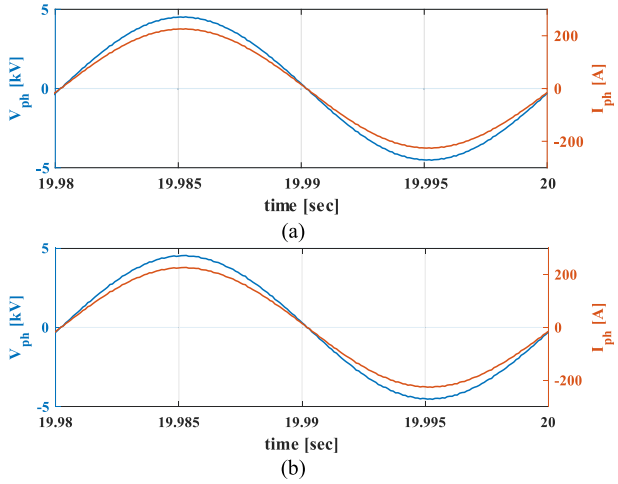

Fig. 5. Output phase voltage and current waveform with a small low-pass filter in the output to filter out the higher harmonics. (a) Balanced system with $\mathbf{\Delta_a} = 0$. (b) Imbalanced system with $\mathbf{\Delta_a} = 0.02$.

performance is superior particularly in case of imbalance. The proposed method requires only two voltage sensors per phase (six for three phases) instead of one per module ($6N$ for three phases), which is on par with other state-of-the-art methods, and compared to the conventional methods, it can reduce the number of sensors from $2N$ to only 2 per phase. We also present a compensation method for lower sampling frequency that can significantly help in reducing the estimation error.

We use KF as an example of an optimal estimator with confirmed performance and relatively easy implementation. However, the developed model may be also used in combination with other state-of-the-art estimators.

V. SIMULATION AND EXPERIMENTAL RESULTS

A single-phase model with $2 \times 8 = 16$ modules ($N = 8$) and 14 clamping branches verifies the feasibility of the proposed model and studies the general behavior of the system. Additionally, a scaled-down prototype provides proof of concept in an experimental setup. Table IV lists the parameters of the simulation and the experimental systems. The specification of the power modules SEMiX854GB176HDs from Semikron is used for the semiconductors. The switching frequency of each module is 2 kHz and the amplitude of the modulation reference varies in the range of 0.50–0.95. Additionally, the sampling frequency of the KF and the sampling rate for the simulations and the experimental setup are 10 kHz, and the execution rate of the estimator is also maintained at 10 kHz.

A. Simulation Studies

We study the behavior of the estimators under balanced conditions with identical modules and imbalanced conditions with a mismatch between the module capacitances and self-discharging rates. In the second case, a normal distribution ($\mu = 0, \sigma^2 = 1$) is considered for the capacitance and resistance of the modules with $\pm 15\%$ spread from the rated values, with the first module having the lowest capacitance and internal resistance. Additionally, the self-discharge rates of modules 2, 4, 7, and 8 are increased with module 8 having the highest discharge to emulate a worst-case scenario.

Fig. 5(a) and (b) show the phase voltage and current waveforms for balanced and imbalanced systems with $\Delta = 0$ and $\Delta = 0.02$, respectively, which verifies that the output is not affected by the balancing effort.

Fig. 6(a) and (b) show the results of the Kalman filters based on the developed state-space model as well as the conventional model of MMCs per [44]. In Fig. 6(a), yellow color marks the true voltages, blue depicts the results using the conventional MMC model, and red depicts the results from the proposed method. The Kalman filter parameters for both estimators are widely identical. The estimation results confirm that both models are stable. However, while both models converge, the modified state-space model can achieve slightly lower absolute errors even in a completely balanced system. According to Fig. 6(b), the maximum error for the proposed estimator in an ideal system is below 0.5%.

Fig. 7 shows the behavior of the estimator in a heavily imbalanced system with $\Delta_a = 0$. Due to the imbalance and without any balancing effort, the voltages start to diverge. Fig. 7(a) illustrates measured and estimated voltages. Similar to the previous case, both of the estimators converge, but the proposed model tracks the measured voltage more closely. Fig. 7(b) verifies a $>50\%$ improvement in the estimation error compared to the conventional model of the MMC as well as a reduction in the amplitude of the error fluctuations.

The third scenario investigates the behavior of the estimators in the imbalanced system with a nonzero level adjustment sufficient to balance the system (here $\Delta_a = 0.02$). Fig. 8(a) presents the profile of the measured and estimated voltages of the capacitors in one arm. Despite the mismatches in the capacitances as well as different discharge rates, the balancing technique can balance the modules with a very small level adjustment. Since the modules start with completely imbalanced voltages, it takes approximately 8 s for the voltages to fully converge to balanced states. However, it is also possible to increase the balancing speed using higher level adjustments (Δ_a). One of the appeals of using an estimator is to actively control Δ_a to achieve faster or

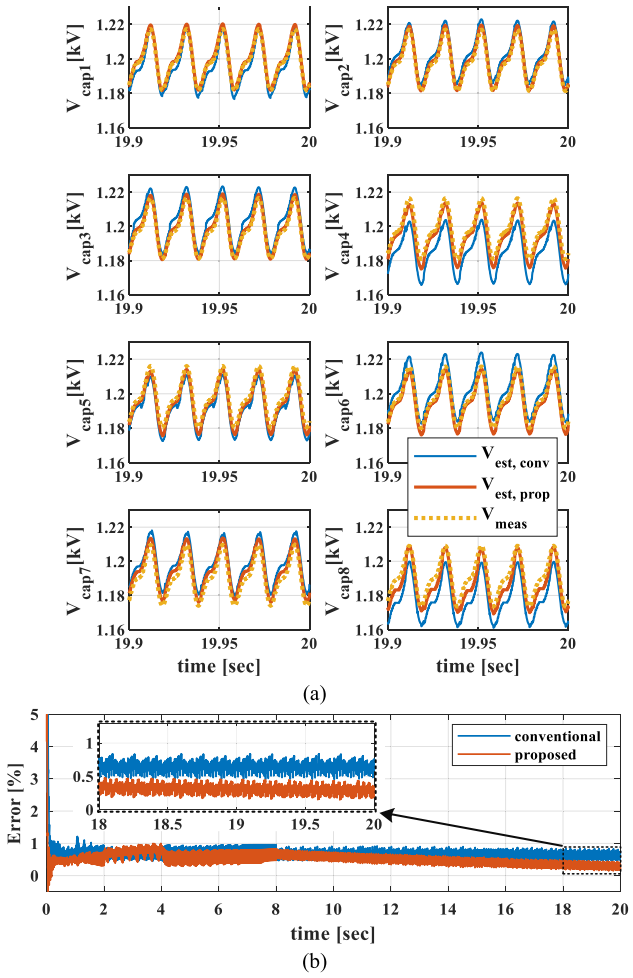

Fig. 6. Simulation results for a balanced system. (a) Estimation of the capacitor voltages for conventional and proposed method. (b) Profile of the maximum estimation error.

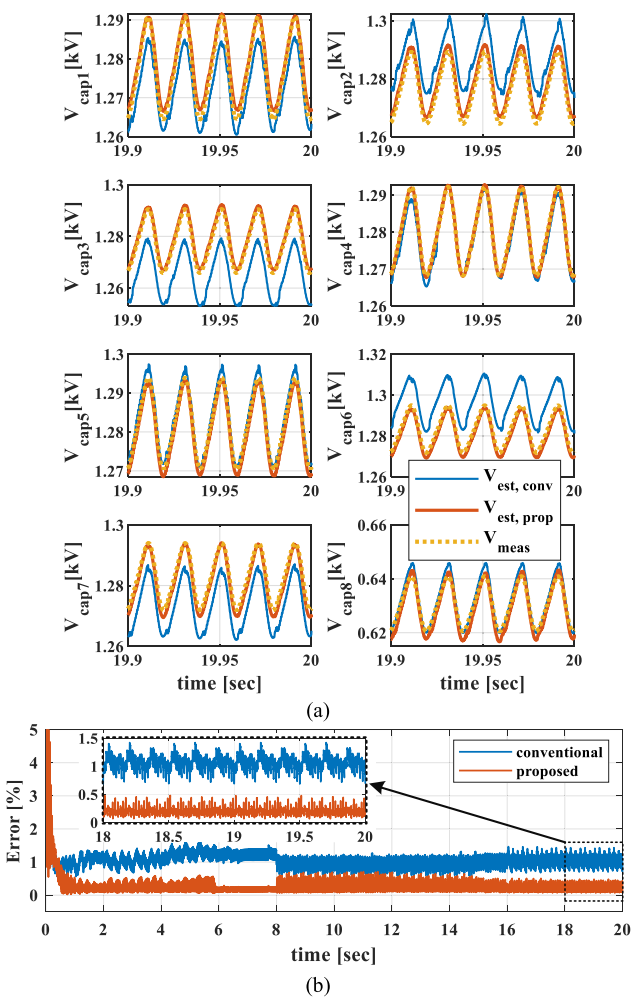

Fig. 7. Simulation results for an imbalanced system without balancing ($\boldsymbol{\Delta_a} = 0$). (a) Estimation of the capacitor voltages for conventional and proposed method. (b) Profile of the maximum estimation error.

more efficient convergences. However, proposing a closed-loop balancer without direct measurement at the modules is out of the scope of this article, as it requires a more in-depth analysis of the balancing factors as well as the balancing efficiency.

Similar to the previous scenarios, the estimator based on the proposed model can track the capacitor voltages with considerably better accuracy. According to Fig. 8, the maximum instantaneous error is <7 V, which is 80% lower compared to the conventional one. The significant increase in the estimation error with a relatively small value of Δ_a shows the sensitivity of the conventional model to the effect of balancing, whereas the proposed compensated model accuracy is more stable and achieves approximately similar results to the previous scenario.

Since normally the individual module switching frequency is low in larger systems, Fig. 9(a) studies the accuracy of the estimators with low-frequency modulation ($f_{\text{sw}} = 200$ Hz) as well as a step variation in the modulation index at $t = 6.5$ s. Additionally, Fig. 9(b) presents the waveform of the estimation errors with a sudden load change at $t = 2.5$ s. The result confirms that the proposed model can easily track the voltage with sufficient accuracy. Lower switching frequencies can lead to slightly higher absolute errors; however, the results are still well below the 1% mark. Additionally, lower modulation indices can increase the average duration that the clamping branch is conducting. Therefore, the compensated model can offer better accuracy and slightly reduce the amplitude of the fluctuations.

Fig. 10 shows the errors of the proposed model as well as the conventional model to the sampling frequency, which also corresponds to the update rate of the estimation algorithm. Each point is the average error for ten-modulation indices ranging from 0.1 to 1, and $\Delta_a = 0$. With reducing the sampling frequency, the error increases. However, due to the developed sampling compensation technique, the proposed model can achieve significantly better results. For example, reducing the update frequency from 10 kHz to approximately 2 kHz results in approximately 1% deterioration in estimation accuracy. The difference further increases with increasing Δ_a.

As seen, in all scenarios the proposed model outperforms the conventional one with a 30%–50% error reduction. Additionally, the proposed method is widely unaffected by level adjustment, lower sampling frequencies, or modulation index variations. For additional results, please see the online supplement.

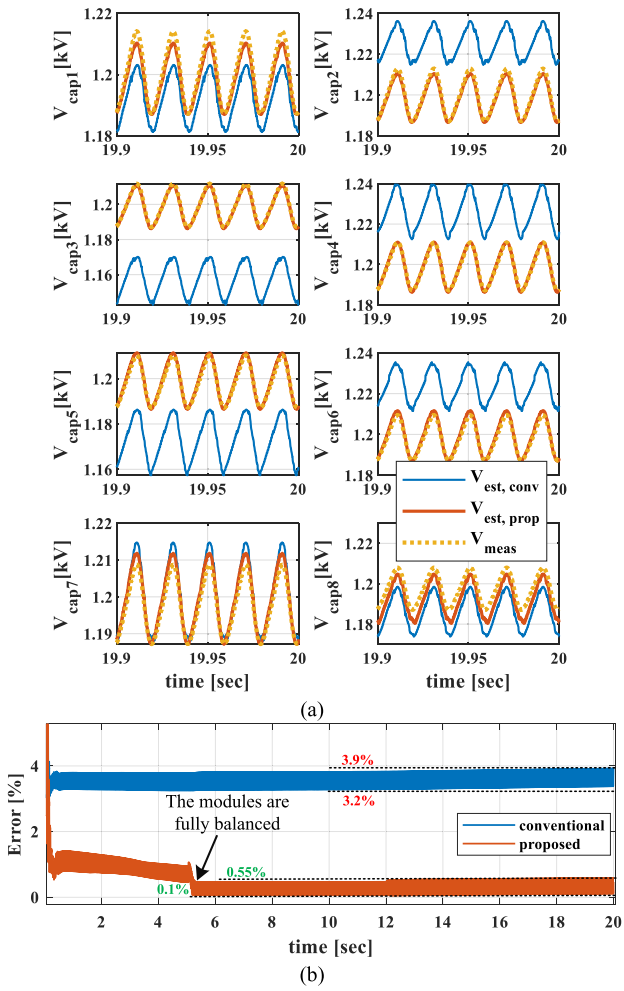

Fig. 8. Simulation results for an imbalanced system with $\boldsymbol{\Delta_a} = 0.02$. (a) Estimation of the capacitor voltages for conventional and proposed method. (b) Profile of the maximum estimation error.

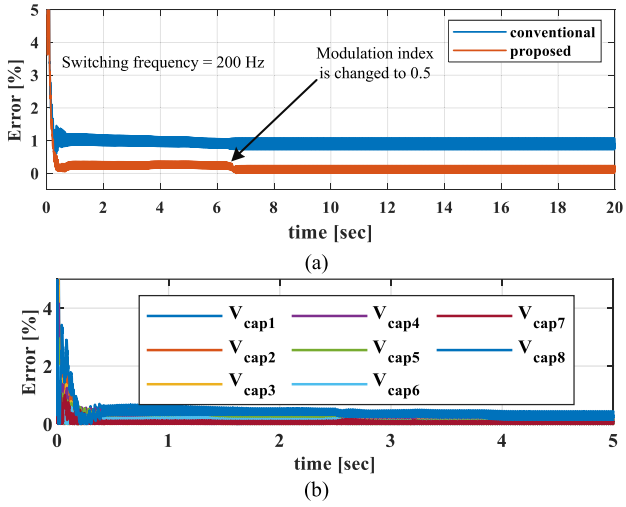

Fig. 9. Profile of estimation error under varying conditions. (a) Maximum error with $\Delta_a = 0$, low-frequency modulation, and step change in modulation index. (b) Estimation errors for a step change in load and PF variations.

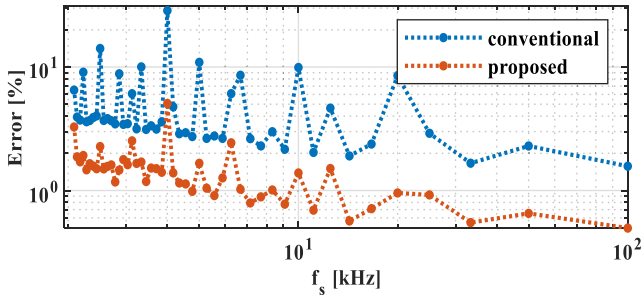

Fig. 10. Profile of the average error with respect to the sampling frequency.

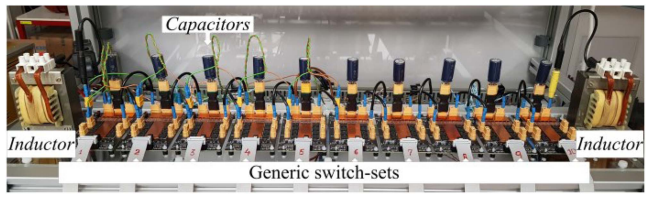

Fig. 11. Picture of the diode-clamped MMC prototype.

B. Experiments

A scaled-down diode-clamped MMC with ten modules verifies the estimator's performance, and Fig. 11 shows a photo of the setup. Each module includes about 500 μF low-ESR ceramic capacitors in parallel with 2.2 mF electrolytic ones. Labview in combination with an FPGA development board (National Instruments sbRIO 9627) performs the control functions and records states for further analysis. Additionally, the voltages of the modules of the upper arm are independently monitored using an oscilloscope to evaluate the estimation accuracy. The measured and estimated voltages are then plotted and analyzed in MATLAB.

Fig. 12(a) shows the estimated and measured arm voltages as well as the estimation error in an imbalanced system for $\Delta_a = 0$. As the effective switching frequency is 10 kHz and the fundamental frequency of the output voltage is 50 Hz, a low-pass with a cut-off frequency of 2 kHz can easily reduce the measurement noise. The maximum error after removing the switching noise from the measurements is 4 V, which corresponds to less than 2% and verifies the capability of the proposed method. Additionally, Fig. 12(b) depicts the measured and estimated capacitor voltages in addition to the estimation error. The maximum estimation error is below 3.5%. Since in this case, the level adjustment is zero, the capacitor voltages do not completely balance, even though the clamping branch ensures that $V_{c1} \geq V_{c2} \geq V_{c3} \geq V_{c4} \geq V_{c5}$.

The balancing behavior as well as the performance of the estimator with nonzero circulating current for $\Delta_a = 0.02$ are shown in Fig. 13. With $\Delta_a = 0.02$, the voltages converge to 45 V and the system has a stable operation after reaching its steady-state condition. The maximum estimation error, in this case, is also below 2%, which confirms the accuracy of the proposed model in combination with the Kalman filter estimator. For additional measurements, see Supplementary Material.

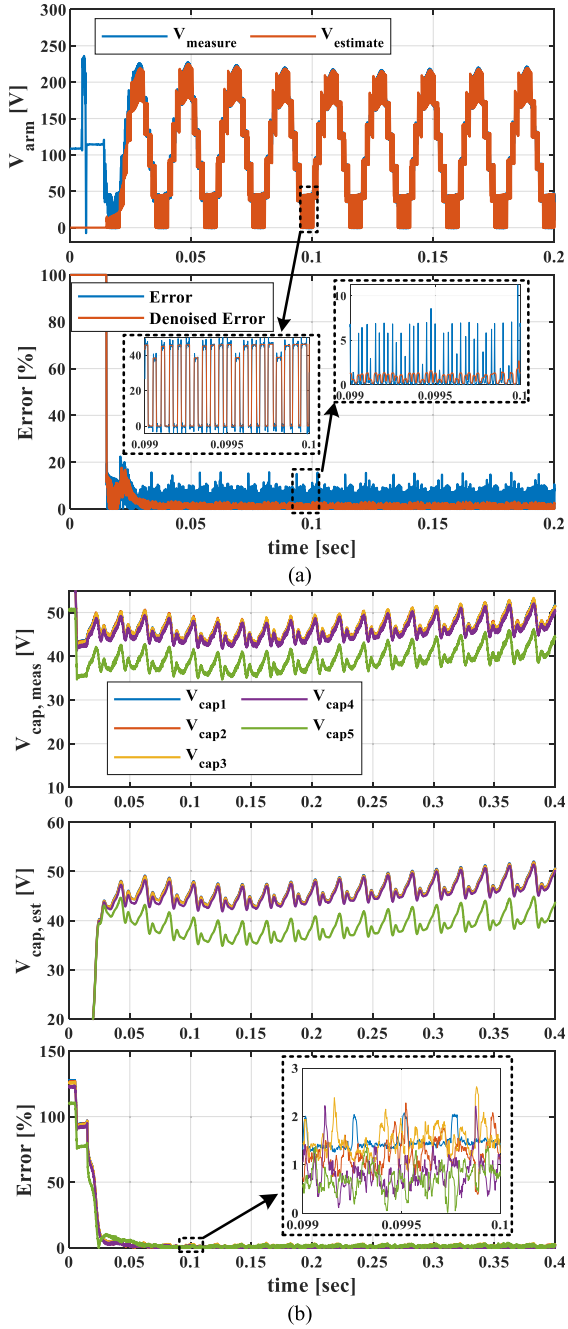

Fig. 12. Results for $\boldsymbol{\Delta_a} = 0$. (a) Measured and estimated arm voltage, as well as error of the arm voltage estimation. (b) Capacitor voltages and estimation results as well as the maximum estimation error.

VI. Conclusion

This article proposes a state-space model for diode-clamped MMCs, which is applicable for the available sensorless balancing techniques for this topology. Additionally, it provides a procedure to use an optimal estimator to achieve sensorless operation at the module levels, while still fully tracking the module voltages. The provided analysis as well as the simulation and experimental results verify the superiority of the developed model compared to the conventional MMC model.

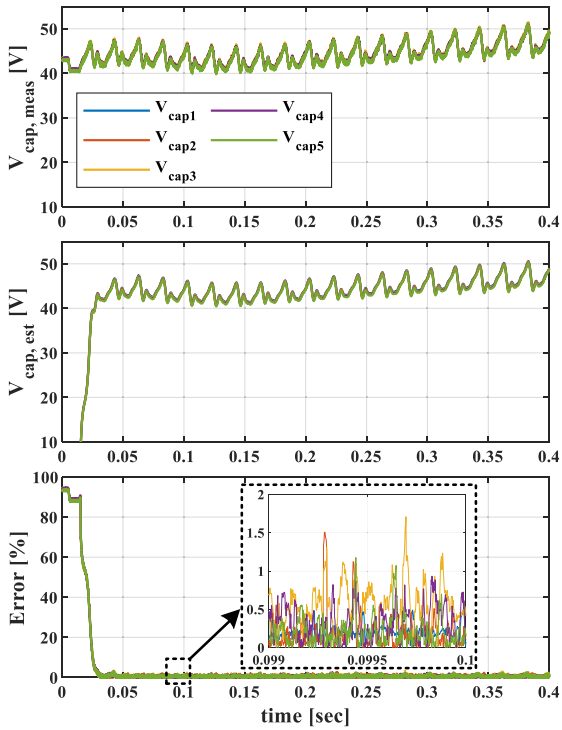

Fig. 13. Estimation results of imbalanced system with $\boldsymbol{\Delta_a} = 0.02$.

The synopsis in Table III clearly highlights significant advantages over the state-of-the-art, and a comparison of the results from the proposed model with the ones from the conventional MMC shows 30%–50% reduction in estimation error. The improvement is even more noticeable in imbalanced systems and/or with larger balancing currents.

The low sampling compensation technique can allow for further reduction of the sampling frequency as well as better sensitivity to the small balancing efforts that might have been neglected in the conventional models with lower sampling frequencies.

Based on the experiments, the estimator can achive accuracies $\geq$97.5% at all times with a wide range of Δ_a= [0, 0.04] and considering a 15% tolerance in the capacitances of the modules. Additionally, in a single-phase system, the estimator can reduce the number of voltage sensors from $2N$ (one voltage sensor per module) to only two sensors (arm voltage sensors).

Although a closed-loop balancer is not the main focus of this article, the proposed model and estimator can be used to achieve a more optimized closed-loop balancing in diode-clamped MMCs without any direct measurement at the module level, and it can minimize the balancing losses in the system.

References

[1] G. Konstantinou, H. R. Wickramasinghe, C. D. Townsend, S. Ceballos, and J. Pou, "Estimation methods and sensor reduction in modular multilevel converters: A review," in *Proc. 8th Int. Conf. Power Energy Syst.*, 2018, pp. 23–28.

[2] S. Wang, T. Dragicevic, Y. Gao, and R. Teodorescu, "Neural network based model predictive controllers for modular multilevel converters," *IEEE Trans. Energy Convers.*, vol. 36, no. 2, pp. 1562–1571, Jun. 2021.

[3] N. Tashakor and M.-H. Khooban, "An interleaved Bi-directional AC–DC converter with reduced switches and reactive power control," *IEEE Trans. Circuits Syst. II, Exp. Briefs*, vol. 67, no. 1, pp. 132–136, Jan. 2020.

[4] C. Wang, F. R. Lizana, Z. Li, A. V. Peterchev, and S. M. Goetz, "Submodule short-circuit fault diagnosis based on wavelet transform and support vector machines for modular multilevel converter with series and parallel connectivity," in *Proc. 43rd Annu. Conf. IEEE Ind. Electron. Soc.*, 2017, pp. 3239–3244.

[5] J. Fang, H. Deng, N. Tashakor, F. Blaabjerg, and S. M. Goetz, "State-space modeling and control of grid-tied power converters with capacitive/battery energy storage and grid-supportive services," *IEEE J. Emerg. Sel. Topics Power Electron.*, vol. 11, no. 1, pp. 234–250, Feb. 2023.

[6] Q. Xiao et al., "A novel fault-tolerant control method for modular multilevel converter with an improved phase disposition level-shifted PWM," in *Proc. 45th Annu. Conf. IEEE Ind. Electron. Soc.*, 2019, pp. 3839–3844.

[7] C. Wang, L. Xiao, C. Wang, M. Xin, and H. Jiang, "Analysis of the unbalance phenomenon caused by the PWM delay and modulation frequency ratio related to the CPS-PWM strategy in an MMC system," *IEEE Trans. Power Electron.*, vol. 34, no. 4, pp. 3067–3080, Apr. 2019.

[8] S. Ali, Z. Ling, K. Tian, and Z. Huang, "Recent advancements in submodule topologies and applications of MMC," *IEEE J. Emerg. Sel. Topics Power Electron.*, vol. 9, no. 3, pp. 3407–3435, Jun. 2021.

[9] K. Ilves, L. Harnefors, S. Norrga, and H.-P. Nee, "Analysis and operation of modular multilevel converters with phase-shifted carrier PWM," *IEEE Trans. Power Electron.*, vol. 30, no. 1, pp. 268–283, Jan. 2015.

[10] N. Tashakor, F. Iraji, and S. M. Goetz, "Low-frequency scheduler for optimal conduction loss in series/parallel modular multilevel converters," *IEEE Trans. Power Electron.*, vol. 37, no. 3, pp. 2551–2561, Mar. 2022.

[11] T. Zheng et al., "A novel Z-type modular multilevel converter with capacitor voltage self-balancing for grid-tied applications," *IEEE Trans. Power Electron.*, vol. 36, no. 2, pp. 1399–1411, Feb. 2021.

[12] T. Zheng et al., "A novel high-voltage DC transformer based on diode-clamped modular multilevel converters with voltage self-balancing capability," *IEEE Trans. Ind. Electron.*, vol. 67, no. 12, pp. 10304–10314, Dec. 2020.

[13] N. Tashakor, M. Kilictas, J. Fang, and S. M. Goetz, "Switch-clamped modular multilevel converters with sensorless voltage balancing control," *IEEE Trans. Ind. Electron.*, vol. 68, no. 10, pp. 9586–9597, Oct. 2021.

[14] Y. Jin et al., "A novel submodule voltage balancing scheme for modular multilevel cascade converter—Double-star chopper-cells (MMCC-DSCC) based STATCOM," *IEEE Access*, vol. 7, pp. 83058–83073, 2019.

[15] K. T. Kosmowski, *Functional Safety and Reliability Analysis Methodology for Hazardous Industrial Plants*. Gdańsk, Poland: Gdańsk Univ. Technol Publishers, 2013.

[16] S. Purewal and M. A. Waldron, "Functional safety in application of programmable devices in power system protection and automation," in *Proc. Int. Eng. Technol. Conf. Proc.*, 2004, pp. 295–298.

[17] A. Nardi and A. Armato, "Functional safety methodologies for automotive applications," in *Proc. IEEE/ACM Int. Conf. Comput.-Aided Des.*, 2017, pp. 970–975.

[18] X. Shi, S. Filizadeh, and A. Gole, "Capacitor energy storage requirements in mixed-submodule hybrid cascaded MMCs," *IEEE Trans. Energy Convers.*, vol. 35, no. 3, pp. 1638–1647, Sep. 2020.

[19] J. Fang, S. Yang, H. Wang, N. Tashakor, and S. Goetz, "Reduction of MMC capacitances through parallelization of symmetrical half-bridge submodules," *IEEE Trans. Power Electron.*, vol. 36, no. 8, pp. 8907–8918, Aug. 2021.

[20] G. Lu, C. Gao, and X. Li, "Voltage self-balance method for series connected IGBTs by using clamping diodes," in *Proc. 43rd Annu. Conf. IEEE Ind. Electron. Soc.*, 2017, pp. 5000–5005.

[21] C. Gao, X. Jiang, Y. Li, Z. Chen, and J. Liu, "A DC-link voltage self-balance method for a diode-clamped modular multilevel converter with minimum number of voltage sensors," *IEEE Trans. Power Electron.*, vol. 28, no. 5, pp. 2125–2139, May 2013.

[22] N. Tashakor, B. Arabsalmanabadi, L. O. Cervera, E. Hosseini, K. Al-Haddad, and S. Goetz, "A simplified analysis of equivalent resistance in modular multilevel converters with parallel functionality," in *Proc. 46th Annu. Conf. IEEE Ind. Electron. Soc.*, 2020, pp. 4158–4163.

[23] J. Fang, F. Blaabjerg, S. Liu, and S. M. Goetz, "A review of multilevel converters with parallel connectivity," *IEEE Trans. Power Electron.*, vol. 36, no. 11, pp. 12468–12489, Nov. 2021.

[24] C. Gao and J. Lv, "A new parallel-connected diode-clamped modular multilevel converter with voltage self-balancing," *IEEE Trans. Power Del.*, vol. 32, no. 3, pp. 1616–1625, Jun. 2017.

[25] J. Xu, M. Feng, H. Liu, S. Li, X. Xiong, and C. Zhao, "The diode-clamped half-bridge MMC structure with internal spontaneous capacitor voltage parallel-balancing behaviors," *Int. J. Elect. Power Energy Syst.*, vol. 100, pp. 139–151, 2018.

[26] X. Liu et al., "A novel diode-clamped modular multilevel converter with simplified capacitor voltage-balancing control," *IEEE Trans. Ind. Electron.*, vol. 64, no. 11, pp. 8843–8854, Nov. 2017.

[27] H. Bahamonde, S. Rivera, Z. Li, S. Goetz, A. Peterchev, and L. F. R., "Different parallel connections generated by the modular multilevel series/parallel converter: An overview," in *Proc. 45th Annu. Conf. IEEE Ind. Electron. Soc.*, 2019, pp. 6114–6119.

[28] G. Guo et al., "HB and FB MMC based onshore converter in series-connected offshore wind farm," *IEEE Trans. Power Electron.*, vol. 35, no. 3, pp. 2646–2658, Mar. 2020.

[29] T. Zheng, C. Gao, X. Liao, X. Liu, B. Sun, and J. Lv, "A medium-voltage motor drive based on diode-clamped modular multilevel converters," in *Proc. 20th Int. Conf. Elect. Mach. Syst.*, 2017, pp. 1–6.

[30] N. Tashakor, D. Keshavarzi, S. Banana, and S. Goetz, "Voltage estimation for diode-clamped MMCs based on a simplified neural network," in *Proc. 24th Eur. Conf. Power Electron. Appl.*, 2022, pp. 1–10.

[31] M. Asoodar, M. Nahalparvari, C. Danielsson, R. Söderström, and H.-P. Nee, "Online health monitoring of DC-link capacitors in modular multilevel converters for FACTS and HVDC applications," *IEEE Trans. Power Electron.*, vol. 36, no. 12, pp. 13489–13503, Dec. 2021.

[32] N. Tashakor, D. Keshavarzi, F. Iraji, S. Banana, and S. Goetz, "Voltage estimation in combination with level-adjusted phase-shifted-carrier modulation (LA-PSC) for sensorless balancing of diode-clamped modular multilevel converters (MMCs)," *IEEE Trans. Power Electron.*, vol. 38, no. 4, pp. 4267–4278, Apr. 2023.

[33] G. Pizarro, P. Poblete, G. Droguett, J. Pereda, and F. Núñez, "Extended Kalman filtering for full-state estimation and sensor reduction in modular multilevel converters," *IEEE Trans. Ind. Electron.*, vol. 70, no. 2, pp. 1927–1938, Feb. 2023.

[34] C. Burgos-Mellado et al., "Cyber-attacks in modular multilevel converters," *IEEE Trans. Power Electron.*, vol. 37, no. 7, pp. 8488–8501, Jul. 2022.

[35] M. Nahalparvari et al., "DC-side impedance estimation of a modular multilevel converter through system identification of a partially black-boxed control system," *IEEE Trans. Energy Convers.*, vol. 37, no. 4, pp. 2708–2721, Dec. 2022.

[36] T. Yin, Y. Wang, X. Wang, S. Yin, S. Sun, and G. Li, "Modular multilevel converter with capacitor voltage self-balancing using reduced number of voltage sensors," in *Proc. Int. Power Electron. Conf.*, 2018, pp. 1455–1459.

[37] F. Rong, X. Gong, X. Li, and S. Huang, "A new voltage measure method for MMC based on sample delay compensation," *IEEE Trans. Power Electron.*, vol. 33, no. 7, pp. 5712–5723, Jul. 2018.

[38] M. Abdelsalam, S. Tennakoon, H. Diab, and M. I. Marei, "An ADALINE based capacitor voltage estimation algorithm for modular multilevel converters," in *Proc. 19th Int. Symp. Elect. App. Technol.*, 2016, pp. 1–4.

[39] A. A. Taffese, E. De Jong, S. D'Arco, and E. Tedeschi, "Online parameter adjustment method for arm voltage estimation of the modular multilevel converter," *IEEE Trans. Power Electron.*, vol. 34, no. 12, pp. 12491–12503, Dec. 2019.

[40] S. Langarica et al., "Denoising and voltage estimation in modular multilevel converters using deep neural-networks," *IEEE Access*, vol. 8, pp. 207973–207981, 2020.

[41] N. Tashakor, B. Arabsalmanabadi, F. Naseri, and S. Goetz, "Low-cost parameter estimation approach for modular converters and reconfigurable battery systems using dual-Kalman-filter," *IEEE Trans. Power Electron.*, vol. 37, no. 6, pp. 6323–6334, Jun. 2022.

[42] N. Tashakor, M. Kilictas, E. Bagheri, and S. Goetz, "Modular multilevel converter with sensorless diode-clamped balancing through level-adjusted phase-shifted modulation," *IEEE Trans. Power Electron.*, vol. 36, no. 7, pp. 7725–7735, Jul. 2021.

[43] H. Shu, S. Lei, and X. Tian, "A new topology of modular multilevel converter with voltage self-balancing ability," *IEEE Access*, vol. 7, pp. 184786–184796, 2019.

[44] O. S. H. M. Abushafa, M. S. A. Dahidah, S. M. Gadoue, and D. J. Atkinson, "Submodule voltage estimation scheme in modular multilevel converters with reduced voltage sensors based on Kalman filter approach," *IEEE Trans. Ind. Electron.*, vol. 65, no. 9, pp. 7025–7035, Sep. 2018.

[45] T. Ghanbari, E. Farjah, F. Naseri, N. Tashakor, H. Givi, and R. Khayam, "Solid-state capacitor switching transient limiter based on Kalman filter algorithm for mitigation of capacitor bank switching transients," *Renewable Sustain. Energy Rev.*, vol. 90, pp. 1069–1081, 2018.

[46] S. D. Brown and S. C. Rutan, "Adaptive Kalman filtering," *J. Res. Nat. Bur. Standards*, vol. 90, no. 6, pp. 403–407, 1985.
[47] H. Givi, E. Hosseini, and E. Farjah, "Estimation of batteries voltages and resistances in modular multilevel converter with half-bridge modules using modified PSO algorithm," in *Proc. 12th Power Electron., Drive Syst., Technol. Conf.*, 2021, pp. 1–7.
[48] B. Arabsalmanabadi, N. Tashakor, Y. Zhang, K. Al-Haddad, and S. Goetz, "Parameter estimation of batteries in MMCs with parallel connectivity using PSO," in *Proc. 47th Annu. Conf. IEEE Ind. Electron. Soc.*, 2021, pp. 1–6.
[49] S. D. Arco and J. A. Suul, "Estimation of sub-module capacitor voltages in modular multilevel converters," in *Proc. 15th Eur. Conf. Power Electron. Appl.*, 2013, pp. 1–10.
[50] A. A. Taffese, E. de Jong, S. D'Arco, and E. Tedeschi, "Online parameter adjustment method for arm voltage estimation of the modular multilevel converter," *IEEE Trans. Power Electron.*, vol. 34, no. 12, pp. 12491–12503, Dec. 2019.
[51] Y. Liu and F. Z. Peng, "A modular multilevel converter with self voltage balancing -part I: Mathematical proof," *IEEE J. Emerg. Sel. Topics Power Electron.*, vol. 8, no. 2, pp. 1126–1133, Jun. 2020.
[52] O. S. M. Abushafa, S. M. Gadoue, M. S. A. Dahidah, D. J. Atkinson, and P. Missailidis, "Capacitor voltage estimation scheme with reduced number of sensors for modular multilevel converters," *IEEE J. Emerg. Sel. Topics Power Electron.*, vol. 6, no. 4, pp. 2086–2097, Dec. 2018.
[53] R. Chakraborty, J. Samantaray, A. Dey, and S. Chakrabarty, "Capacitor voltage estimation of MMC using a discrete-time sliding mode observer based on discrete model approach," *IEEE Trans. Ind. Appl.*, vol. 58, no. 1, pp. 494–504, Jan./Feb. 2022.
[54] G. Pizarro, P. M. Poblete, G. Droguett, J. Pereda, and F. Nunez, "Extended Kalman filtering for full state estimation and sensor reduction in modular multilevel converters," *IEEE Trans. Ind. Electron.*, vol. 70, no. 2, pp. 1927–1938, Feb. 2023.
[55] Z. Wang and L. Peng, "Grouping capacitor voltage estimation and fault diagnosis with capacitance self-updating in modular multilevel converters," *IEEE Trans. Power Electron.*, vol. 36, no. 2, pp. 1532–1543, Feb. 2021.
[56] M. D. Islam, R. Razzaghi, and B. Bahrani, "Arm-sensorless sub-module voltage estimation and balancing of modular multilevel converters," *IEEE Trans. Power Del.*, vol. 35, no. 2, pp. 957–967, Apr. 2020.